ACS Macro Letters

Letter

pubs.acs.org/macroletters

Dual-Modal Tumor Imaging via Long-Circulating Biodegradable Core-Cross-Linked Polymeric Micelles

Jun Zhao,[†] Shaoli Song,[†,‡] Meng Zhong, and Chun Li*

Department of Experimental Diagnostic Imaging, The University of Texas, MD Anderson Cancer Center, 1515 Holcombe Blvd., Houston, Texas 77030, United States

Supporting Information

ABSTRACT: We present a long-circulating biodegradable core-cross-linked polymeric micelle (d-CCPM) for the nuclear/optical imaging of tumors. The d-CCPM was derived from an amphiphilic block-copolymer consisting of a hydrophilic block of brush-like poly(ethylene glycol) and a hydrophobic block containing cleavable pendant triethoxysilane. The resultant imaging tracer had prolonged circulation in the blood (half-life of clearance phase = 36.5 h), substantial accumulation in tumors (% injected dose per gram of tissue = 8.5% ± 1.0% at 24 h postinjection), and minimal uptake in the liver (5.0% ± 0.1%) or spleen (5.1% ± 0.3%). Both nuclear and near-infrared fluorescence (NIRF) imaging revealed strong signals in tumor regions. At 48 h, nuclear imaging exhibited tumor-to-liver and tumor-to-blood ratios of 1.4 and 1.1, respectively. The degradation of d-CCPM was studied in vitro at pH 5.0 and 37 °C and confirmed by transmission electron microscopy. Our study indicates that the d-CCPM system is an effective probe for dual-modal cancer imaging and a potential safe platform nanocarrier for the delivery of anticancer drugs and cancer therapy.

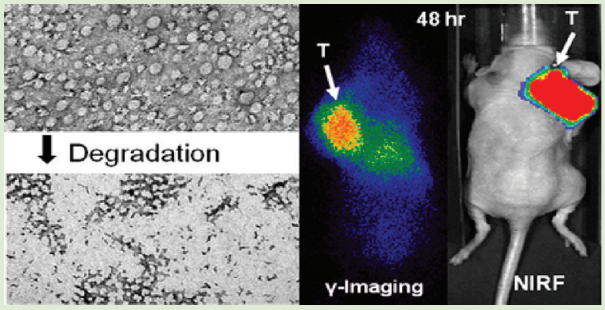

Single-modal imaging tracers can hardly meet the complex requirements of modern tumor imaging, such as target specificity, high sensitivity, high spatial resolution, sufficient tissue penetration, and three-dimensional tomography.[1] Multiple imaging tracers incorporated into one nanoparticle, on the other hand, are able to integrate the merits of individual components and compensate for their deficiencies. The nanoparticle platform can be further tailored to obtain desirable pharmacokinetics and minimal nontumor uptake by optimizing the size and surface properties.[2] The passive accumulation of nanoparticles in tumors is achieved via the enhanced permeation and retention (EPR) effect due to the leaky vascular structures and lack of lymphatic drainage in tumor tissue.[3] The tumor uptake of nanoparticles can be augmented using targeting ligands such as folic acid and some tumor-specific peptides.[4−7] Nevertheless, prolonged circulation is still favorable because it increases the residential time of targeting ligands that pass through the tumor and become recognized by the targets.[8] However, many imaging tracers currently under investigation still exhibited a short circulation half-life; their entrapment in the liver and spleen consumed a significant part of the injected dose.[9−13]

Recently we reported a core-cross-linked polymeric micelle (CCPM) system with a prolonged blood circulation and low uptake in the liver or spleen.[14] These qualities were probably due to the cross-linked core that prevented the premature micelle disintegration in vivo. Also, the brush-like poly(ethylene glycol) (PEG) formed a dense protective layer on the micelle surface and minimized the micelle uptake in the reticuloendothelial system (RES). Lastly, the micelle size (24 ± 8.9 nm) was above the threshold of renal clearance yet not so large as to be captured by the RES.[15] However, this CCPM lacked biodegradability and might pose health hazards for long-term applications. Degradable polymeric micelles have been developed by incorporating cleavable linkages into the polymer backbone or pendant groups.[16,17]

In this study we successfully introduced biodegradability into the cross-linker of the CCPM system without compromising its merits in biodistribution, pharmacokinetics, or imaging quality. The preparation of this degradable CCPM (d-CCPM) is illustrated in Scheme 1. The polymer precursor consisted of a hydrophilic block of brush-like PEG, as well as a hydrophobic block containing pendant triethoxysilane through a degradable succinic ester bond. Micelles were formed spontaneously upon the slow addition of water into the methanol solution of the copolymer and a near-infrared fluorescent (NIRF) fluorophore, 3-triethoxysilyl-propyl IR783 (NIRFSi). The cross-linking followed the hydrolysis and condensation of triethoxysilane, while NIRFSi was simultaneously loaded into d-CCPM at 0.2% wt. The d-CCPM was then purified via dialysis and filtration. The fluorescence emission spectrum of d-CCPM in PBS (pH 7.4) exhibited a maxima at 831 nm (λ_{ex} = 765 nm, see Figure S3 in the Supporting Information, SI). The surface amine of d-CCPM was conjugated to a metal chelator, diethylenetriamine pentaacetic acid (DTPA), to enable the radiolabeling with ^{111}In

Received: August 22, 2011
Accepted: December 5, 2011
Published: December 8, 2011

   dx.doi.org/10.1021/mz200034f | *ACS Macro Lett.* 2012, 1, 150−153

Scheme 1. Synthesis and Degradation of CCPM Loaded with Radioisotope ^{111}Indium and NIRF Dye. The Detailed Structure of the Crosslinking Silica Cluster Is Illustrated in the Inset

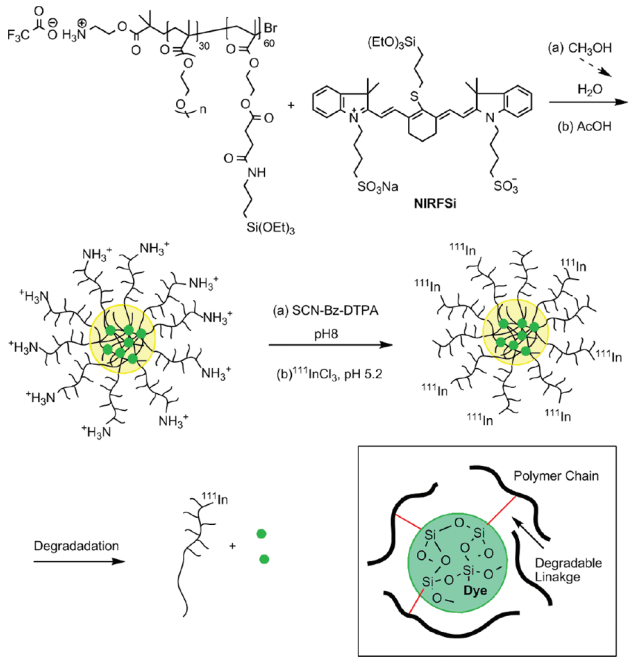

at 195 μCi/mg of micelles. The radiolabeling efficiency was 94% (Figure S5 of the SI). The radiolabeling was quite stable. When ^{111}In-labeled d-CCPM was incubated in mouse whole blood at 37 °C, no significant dissociation of ^{111}In from d-CCPM was observed after 7 days of incubation (Figure S6 of the SI).

The average hydrodynamic diameter of d-CCPM was 25.2 nm with a narrow size distribution (PDI = 0.037, Figure 1A). Similar results were observed in the transmission electron microscopy (TEM) image (Figure 1B). The micelles were hydrolyzed by the scission of succinic ester bonds between the silica clusters and the surrounding polymer backbones (see the inset of Scheme 1). The succinic ester bond is known to be susceptible to hydrolysis in acidic environments, for example, lysosomes.[18−20] Disintegrated d-CCPM was observed after 1 week of incubation in a pH 5.0 buffer at 37 °C (Figure 1C). In contrast, the nondegradable CCPM, in which the pendant triethoxysilane was linked through a nondegradable bond to the backbone of the hydrophobic block, remained intact under a harsher condition (0.1 M HCl, Figure 1D).

The d-CCPM had low cytotoxicity to human liver carcinoma (Hep-G2) and human embryonic kidney 293 (HEK-293) cell lines. No significant toxicity was found in either cell line as the micelle concentration increased from 10 to 1000 μg/mL (Figure 2).

All animal studies were carried out in accordance to institutional animal care and use guidelines. In vivo pharmacokinetics was evaluated in female BALB/c mice using ^{111}In-labeled d-CCPM. The blood activity−time profile (Figure 3A) fits well into a two-compartment model described by the equation:[21]

$$Ct(\%\mathrm{ID/g}) = Ae^{-\alpha t} + Be^{-\beta t}$$

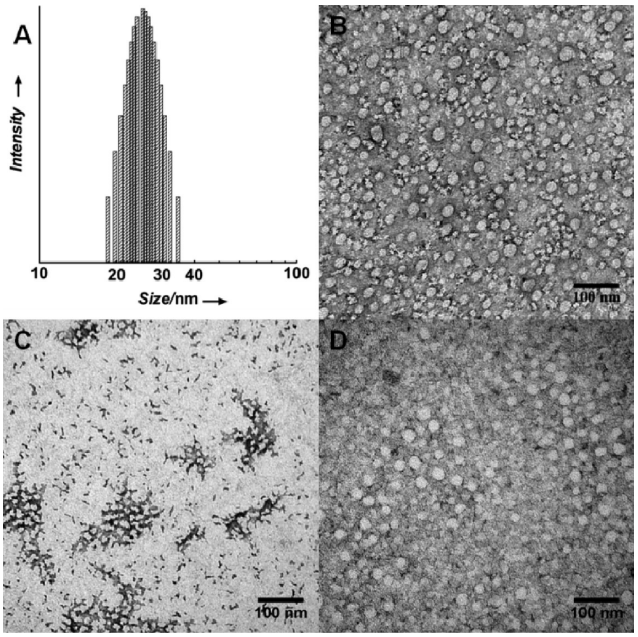

Figure 1. (A) Dynamic light scattering (DLS) histogram and (B) TEM image of d-CCPM prior to degradation; (C) TEM images of disintegrated d-CCPM in pH 5.0 buffer and (D) nondegradable CCPM after 1 week of incubation at 37 °C in 0.1 M HCl.

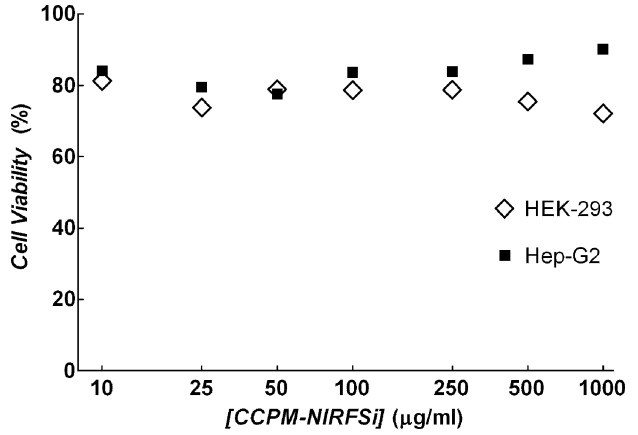

Figure 2. In vitro cell toxicity study of CCPM-NIRFSi using human embryonic kidney (HEK-293) and human liver carcinoma Hep-G2 cell lines. Untreated cells were used as the control. Viability data were normalized against the control groups. All data were presented as mean ± standard deviation (n = 6). The standard deviation values were too small to be visible in the figure.

Based on this equation, the half-life of ^{111}In-labeled d-CCPM was 0.5 h in the distribution phase and 36.5 h in the clearance phase.

Biodistribution data were obtained from nude mice bearing subcutaneous CT-26 tumors at 24 and 48 h post-injection (Figure 3B). The d-CCPM level (%ID/g) in the blood was 15.4 ± 1.5 at 24 h and decreased to 7.5 ± 0.8 at 48 h. RES organs had low uptake at both time points. The liver uptake was 5.0 ± 0.1 and 6.1 ± 0.4, while the spleen uptake was 5.1 ± 0.3 and 6.8 ± 0.3, respectively. CCPM accumulation in tumors at 24 h was 8.5 ± 1.0 and did not change at 48 h (8.5 ± 1.7). Most notably, at 48 h, more d-CCPM resided in tumors than the blood, liver, or spleen, underscoring substantial reduction in RES uptake of d-CCPM. The autoradiograph and fluorescence

dx.doi.org/10.1021/mz200034f | ACS Macro Lett. 2012, 1, 150−153

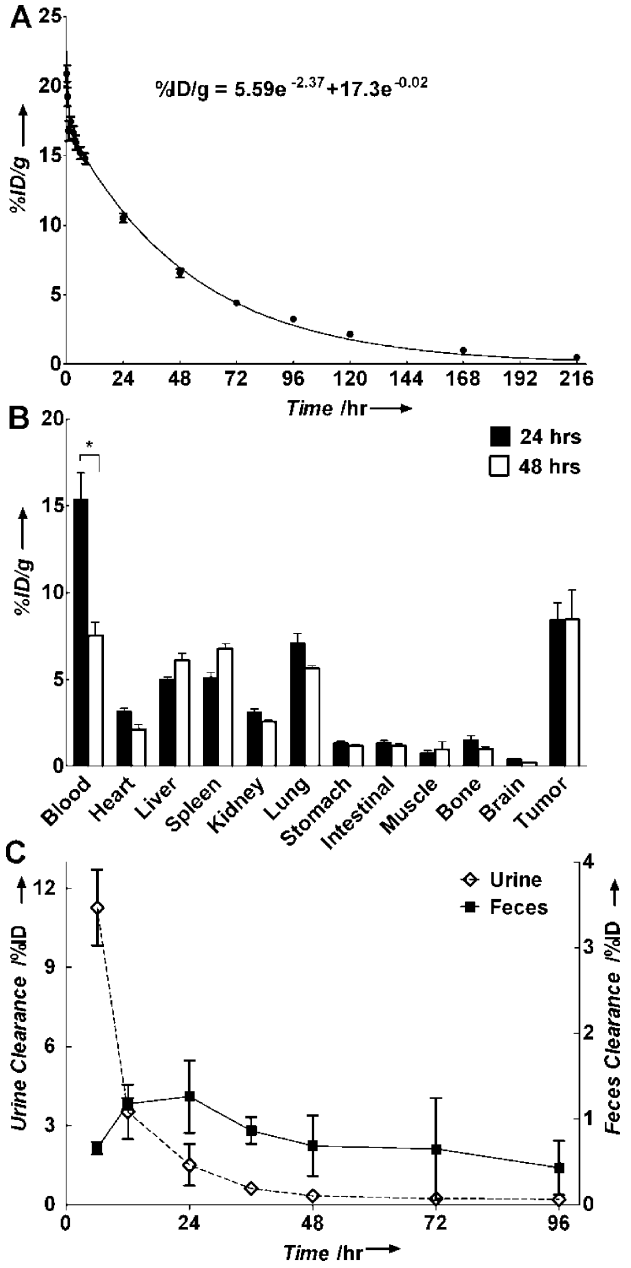

Figure 3. Pharmacokinetics, biodistribution, and whole body clearance studies. (A) Blood activity−time profile. Filled circles represent the mean radioactivity expressed as % injected dose per gram of blood (% ID/g) from 10 mice. The solid line is a curve fitted to a two-compartment model. (B) Biodistribution results obtained from radioactivity count (four mice at each time point), plotted as %ID per gram of tissue. (C) Whole body clearance via urine (open diamond) and feces (filled circle) at each time point were collected from six mice, plotted as % injected dose. All data are expressed as the mean ± standard error.

scanning of tumor slices demonstrated the colocalization of both imaging tracers, suggesting that over the period of the 48 h study both the ^{111}In-labeled backbone and NIRFSi-labeled cross-linking core remained associated with residual d-CCPM (Figure S7 of the SI). Biodistribution data at 72 and 96 h were also recorded (Figure S8 of the SI). Compared to the results at a shorter time, there was a significant increase in liver uptake (%ID/g): 16.7 ± 0.4 at 72 h and 15.6 ± 1.5 at 96 h. Such an increase indicated that degraded d-CCPM was captured by the liver. Uptakes in the spleen, 4.2 ± 0.2 at 72 h and 4.3 ± 0.3 at 96 h, were lower than at earlier time points. Notably, most d-CCPM was cleared from the lung by 72 h. The lung uptake was 0.6 ± 0.1 at both 72 and 96 h, while lung uptakes were 7.1 ± 0.5 and 5.6 ± 0.2 at 24 h and 48 h, respectively.

Radioactivity was detected in both urine and feces post-injection. Considering the excellent stability of radiolabeling, such radioactivity in urine and feces indicated the clearance of d-CCPM (Figure 3C). There was significant urine clearance during the first 6 h (11.3% of injected dose excreted). Similar finding was recorded with nondegradable CCPM.[14] The renal clearance threshold for soft d-CCPM may be higher than hard quantum dots, which was previously determined to be around 5 nm in diameter.[15] The clearance via feces suggested that d-CCPM was degraded in liver and excreted through bile. The clearance study was stopped at 96 h due to the short half-life of ^{111}In. Long-term clearance would require isotopes with longer half-lives.

Figure 4 shows representative images from γ-scintigraphy, single-photon-emission computed tomography (SPECT), and

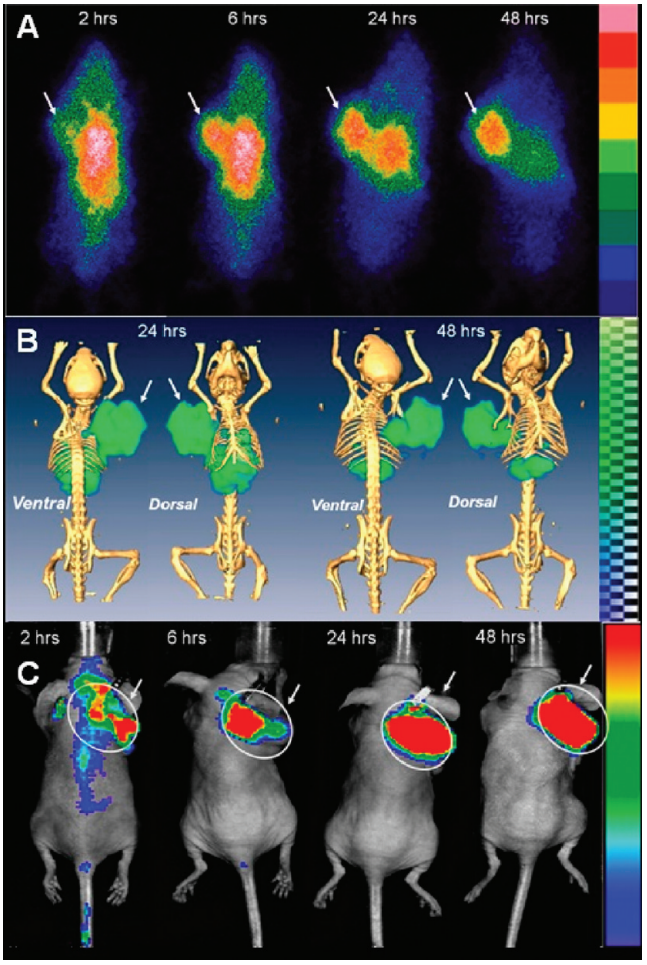

Figure 4. γ-Scintigraphy (A), SPECT (B), and NIRF (C) images post-injection of ^{111}In-d-CCPM. Mice were at dorsal positions in A and ventral positions in C.

NIRF at different time intervals after intravenous injection of ^{111}In-labeled d-CCPM. Micelles were administrated at a dose of 1.0 mg/mouse, corresponding to 195 μCi ^{111}In and 2.1 nmol fluorophore/mouse. The γ-imaging (Figure 4A) results were

dx.doi.org/10.1021/mz200034f | ACS Macro Lett. 2012, 1, 150−153

concordant with the biodistribution data. At 2 h, the blood pool emitted strong signals. The high-uptake areas were the lung, liver, and spleen. The activity from blood pool and background decreased over time, while d-CCPM accumulated in tumors. The tumor was clearly visualized by 24 h post-injection. By 48 h post-injection, there was higher uptake in the tumors than in the liver and the spleen. SPECT mapped the three-dimensional distribution of d-CCPM, which was consistent with the γ-imaging results. NIRF also showed that the tumor uptake increased from 2 to 24 h and remained the same at 48 h (Figure 4C).

In conclusion, we successfully developed a dual-modal imaging tracer using d-CCPM that exhibited degradability, minimal cytotoxicity, prolonged blood circulation, reduced RES uptake, and significant accumulation in tumors. Our study proves that the d-CCPM system is an effective probe for tumor imaging and a potentially safe platform nanocarrier for drug delivery and cancer therapy.

■ ASSOCIATED CONTENT

Ⓢ Supporting Information

Experimental details, images, and spectra. This material is available free of charge via the Internet at http://pubs.acs.org.

■ AUTHOR INFORMATION

Corresponding Author

*Fax: (+1) 713-794-5456. E-mail: cli@mdanderson.org.

Present Address

‡On leave from Department of Nuclear Medicine, RenJi Hospital, ShangHai JiaoTong University, School of Medicine, Shanghai, China, 200127.

Author Contributions

†These authors contributed equally.

Notes

The authors declare no competing financial interest.

■ ACKNOWLEDGMENTS

We thank Dawn Chalaire for expert editorial assistance and Kenn Dunner for aquiring TEM images. This work was supported by the National Cancer Institute (Grant Nos. R01 CA119387 and RC2 GM092599), National Natural Science Foundation of China (No. 81101073), and the John S. Dunn Foundation. The animal facility at MD Anderson Cancer Center is supported by Cancer Center Support Grant No. CA16672 awarded by the National Cancer Institute. The TEM study was performed in the High-Resolution Electron Microscopy Facility of the MD Anderson Cancer Center and supported by Institutional Core Grant No. CA16672.

■ REFERENCES

(1) Cheon, J.; Lee, J.-H. *Acc. Chem. Res.* **2008**, *41*, 1630.
(2) Torchilin, V. P. *J. Controlled Release* **2001**, *73*, 137.
(3) Maeda, H.; Wu, J.; Sawa, T.; Matsumura, Y.; Hori, K. *J. Controlled Release* **2000**, *65*, 271.
(4) Bhattacharya, S.; Franz, A.; Li, X. L.; Jasti, B. *J. Drug Targeting* **2008**, *16*, 780.
(5) Smith, B. R.; Cheng, Z.; De, A.; Koh, A. L.; Sinclair, R.; Gambhir, S. S. *Nano Lett.* **2008**, *8*, 2599.
(6) Yang, L. L.; Mao, H.; Wang, Y. A.; Cao, Z. H.; Peng, X. H.; Wang, X. X.; Duan, H. W.; Ni, C. C.; Yuan, Q. G.; Adams, G.; Smith, M. Q.; Wood, W. C.; Gao, X. H.; Nie, S. M. *Small* **2009**, *5*, 235.
(7) Lu, W.; Xiong, C.; Zhang, G.; Huang, Q.; Zhang, R.; Zhang, J. Z.; Li, C. *Clin. Cancer Res.* **2009**, *15*, 876.
(8) Li, S.-D.; Huang, L. *Mol. Pharmaceutics* **2008**, *5*, 496.
(9) Chen, L. D.; Liu, J.; Yu, X. F.; He, M.; Pei, X. F.; Tang, Z. Y.; Wang, Q. Q.; Pang, D. W.; Li, Y. *Biomaterials* **2008**, *29*, 4170.
(10) Weissig, V.; Whiteman, K. R.; Torchilin, V. P. *Pharm. Res.* **1998**, *15*, 1552.
(11) Rossin, R.; Pan, D. P. J.; Qi, K.; Turner, J. L.; Sun, X. K.; Wooley, K. L.; Welch, M. J. *J. Nucl. Med.* **2005**, *46*, 1210.
(12) Morille, M.; Montier, T.; Legras, P.; Carmoy, N.; Brodin, P.; Pitard, B.; Benoit, J. P.; Passirani, C. *Biomaterials* **2010**, *31*, 321.
(13) Bhushan, K. R.; Misra, P.; Liu, F.; Mathur, S.; Lenkinski, R. E.; Frangioni, J. V. *J. Am. Chem. Soc.* **2008**, *130*, 17648.
(14) Yang, Z.; Zheng, S. Y.; Harrison, W. J.; Harder, J.; Wen, X. X.; Gelovani, J. G.; Qiao, A.; Li, C. *Biomacromolecules* **2007**, *8*, 3422.
(15) Longmire, M.; Choyke, P. L.; Kobayashi, H. *Nanomedicine* **2008**, *3*, 703.
(16) Sun, H.; Guo, B.; Cheng, R.; Meng, F.; Liu, H.; Zhong, Z. *Biomaterials* **2009**, *30*, 6358.
(17) Talelli, M.; Iman, M.; Varkouhi, A. K.; Rijcken, C. J.; Schiffelers, R. M.; Etrych, T.; Ulbrich, K.; van Nostrum, C. F.; Lammers, T.; Storm, G.; Hennink, W. E. *Biomaterials* **2010**, *31*, 7797.
(18) Pignatello, R.; Paolino, D.; Panto, V.; Pistara, V.; Calvagno, M. G.; Russo, D.; Puglisi, G.; Fresta, M. *Curr. Cancer Drug Targets* **2009**, *9*, 202.
(19) Khandare, J. J.; Jayant, S.; Singh, A.; Chandna, P.; Wang, Y.; Vorsa, N.; Minko, T. *Bioconjugate Chem.* **2006**, *17*, 1464.
(20) Fundueanu, G.; Constantin, M.; Ascenzi, P. *Biomaterials* **2008**, *29*, 2767.
(21) Wen, X.; Wu, Q.-P.; Ke, S.; Wallace, S.; Charnsangavej, C.; Huang, P.; Liang, D.; Chow, D.; Li, C. *Cancer Biother. Radiopharm.* **2003**, *18*, 819.